Journal of Molecular Liquids 380 (2023) 121730

Contents lists available at ScienceDirect

Journal of Molecular Liquids

journal homepage: www.elsevier.com/locate/molliq

Ideal micro-lenticular lens based on phase modulation of optically isotropic liquid crystal-polymer composite with three terminals

Srinivas Pagidi [a,b,c,1], MinSu Kim [b,1], Ramesh Manda [b,d], Soyeon Ahn [a], Min Yong Jeon [a,*], Seung Hee Lee [b,*]

[a] Institute of Quantum Systems (IQS) and Department of Physics, Chungnam National University, 99 Daehak-ro, Yuseong-gu, Daejeon 34134, Republic of Korea
[b] Department of Nano Convergence Engineering and Department of Polymer-Nano Science and Technology, Jeonbuk National University, Jeonju, Jeonbuk 54896, Republic of Korea
[c] Department of Convergence System Engineering and Department of Electrical, Electronics, and Communication Engineering Education, Chungnam National University, 99 Daehak-ro, Yuseong-gu, Daejeon 34134, Republic of Korea
[d] School of Physics, University of Hyderabad, Gachibowli, Hyderabad, Telangana-500046, India

ARTICLE INFO

Article history:
Received 12 October 2022
Revised 21 March 2023
Accepted 24 March 2023
Available online 25 March 2023

Keywords:
Liquid Crystals
nano-PDLC
Phase modulation
Vertical and In-plane switching
Tunable photonic device
Transparent film

ABSTRACT

Optical phase modulation in a transparent polymer film composed of nano-sized liquid crystal (LC) droplets embedded within a polymer matrix exhibits a micro-lenticular lensing effect under controlled in-plane field switching (IPS) with interdigitated electrodes. Despite of the lensing effect, the lens profile does not match ideal one and its effective phase modulation is relatively small owing to the weak field strength over the electrodes, which causes an invariant refractive index in these regions. To achieve ideal lens profile and high phase modulation, a vertical electric field is applied between top plane and bottom interdigitated electrodes, while maintaining the in-plane fields between the bottom interdigitated electrodes. The combined effect, referred to as the vertical and in-plane switching (VIS) mode, can achieve larger phase modulation ($\Delta\delta$) than the IPS mode. Consequently, the proposed micro-lenticular lens has a shorter focal length and a significantly better lens profile, similar to the ideal one. Furthermore, the diffraction efficiency (D_f) is effectively improved by ~ 6.7%, 4%, and 2% for the zeroth (0^{th}), $\pm1^{st}$, and $\pm 2^{nd}$ orders, respectively, compared to those in the IPS mode. The improved phase profile with the proposed micro-lenticular device can be used in a switchable lens from 2-dimensions (2D) to 3-dimension (3D) and tunable diffractors.

1. Introduction

Thus far, the fabrication of flat panel displays and optical devices using liquid crystals (LCs) has been widely utilized owing to its benefits including small and dimensionally stable size, voltage-driven devices with high reliability, and low power consumption. Given these advantages, LC has been utilized in a variety of electro-optic displays [1] and photonic applications such as optical diffusers [2], spatial light modulators [3], Fresnel lenses [4], mirrorless lasers [5], and adaptive optical components [6–11]. In addition, most emerging high-quality mobiles, as well as augmented and virtual reality technologies, require a response time of less than a few milliseconds, which cannot be realized in basic LC modes [12,13]. Switchable lenticular lenses [14–16] and switchable barriers [17–19] have recently received significant attention for achieving three-dimensional (3D) images without the use of headsets. Currently, they play an essential role in developing next-generation display technologies. The switchable LC lenticular lens has been considered as a potential candidate for 2D/3D displays because of its higher transmittance and better resolution than parallax barriers. However, basic switchable LC 2D/3D devices rely on a thin-layer coating of an alignment layer and its rubbing to act on the LC molecules to orient them along a specific direction. This limits the device design freedom and increases fabrication complexity in surface relief structures [20]. The application of external strain/pressure by mechanical bending disturbs the orientation of LC molecules in conventional LC devices, resulting in the distortion of the quality of 3D images being visualized. A thick LC layer is also essential for improving periodic phase modulation and light-controlling power, but it slows down the switching time [21,22]. Furthermore, it has been discovered that achieving a uniform cell gap and traditional LC performances in the emerging flexible modes is an extremely difficult task, and the associated technical challenges restrict their applications.

The use of conventional LC modes to overcome these fundamental difficulties has been confirmed to be challenging. Besides

* Corresponding authors.
E-mail addresses: myjeon@cnu.ac.kr (M.Y. Jeon), lsh1@jbnu.ac.kr (S. Hee Lee).
[1] These authors contributed equally to this paper.

https://doi.org/10.1016/j.molliq.2023.121730
0167-7322/

the traditional LC modes are incompatible with flexibility because of the fluidic nature of LC molecules. Nontrivial systems, such as binary or tertiary LC composite systems, must be explored from the perspective of nano-photonics in the context of conventional LC modes. Nano-PDLCs have a number of unusual properties associated with encapsulated nano-scale LC droplets in a polymer matrix, including an optically isotropic phase and a quick response time [23–25]. Nano-scaled LC droplets (< 300 nm) and their random distribution of bipolar structured LC droplets embedded in a polymer matrix were used to achieve optically isotropic behavior. The induced birefringence is a characteristic of their behavior that results from the collective orientational ordering of LC molecules in response to external cues. It also exhibits a high degree of transparency (86%) and can bend up to 4 mm in radius without affecting the photonic behavior [26]. Furthermore, a well-developed in situ photo-polymerization technique provides further control of the LC droplet architecture, which determines the induced birefringence. Subsequently, the phase modulation of incident light occurs upon reorienting the optically isotropic LC droplets by an external stimulus [13,27]. Several interesting studies on tunable microlenses [28,29], 2D/3D switchable micro-lenticular lenses [30], and tunable gratings [13,26] have recently been conducted using polarization-independent optical phase modulation of optically isotropic nano-PDLCs.

Although nano-PDLCs have been considered as potential candidates for a variety of photonic applications, their low phase modulation under the in-plane field switching (IPS) mode due to the minimal field strength right above the interdigitated electrodes restricts their wide-range commercial applications. Taking a completely different approach in this study, we drive a nano-PDLC by a novel electrode structure that consists of both the vertical and in-plane switching (VIS) modes, where a constant bias voltage is applied between top and bottom electrodes, while an in-plane field is retained in the bottom interdigitated electrodes. With the contribution of VIS fields, we achieve larger phase modulation ($\Delta\delta$) and effective gradient refractive index between electrodes. Therefore, the optical path experience and follow the gradient refractive index, resulting in effective micro-lenticular lensing effect with focal lengths in the range of 38 μm as the polarized incident beam passes perpendicular to the electrodes. Furthermore, the proposed VIS mode exhibits a higher diffraction efficiency (D_f) than the conventional IPS mode. Our proposed VIS mode not only performances as an excellent micro-lenticular lens device but also has the potential to be the best diffractive optical element.

2. Switching mechanism of the micro-lenticular lensing effect

Fig. 1 depicts a schematic switching mechanism based on optical phase modulation of optically isotropic nano-PDLC, where the nano-sized LC droplets embedded in a polymer matrix that can be driven by IPS and VIS fields. The nano-sized LC droplet has a bipolar configuration, with the the LC director following the tangentially anchored molecules at the polymer walls while following a straight line that connects the two poles in the center of the droplet. The proposed device consists of a bottom substrate with interdigitated electrodes and a top substrate with a plane electrode. The interdigitated electrodes over the bottom substrate are denoted by P1 and P2, whereas the top plane electrode is denoted by P3. The switching mechanism causes the patterned electrodes to generate a non-uniform field strength across the device. To fully understand this concept, the entire device area was divided into three major regions: I, II, and III, covering the area directly above the electrodes, the edges of the electrodes, and non-electrodes (dotted lines in Fig. 1). In the field-off state, the device exhibit an optically isotropic phase, i.e. optically transparent in the visible wavelength regime with the refractive index (n_i) because the optical film consists of nano-sized LC droplets with size less than the wavelength of visible light, i.e. 300 nm, and their corresponding LC director of bipolar droplet is randomly oriented with respect to their neighboring droplet [27,31]. For this reason, the optically birefringent film does not experience synchronized phase modulation to optical beam while propagating across all regions of the device, as shown in Fig. 1(a). In this situation, the optically isotropic phase n_i can be written in all regions as [30,32]

$$n_i = v_p n_p + v_{lc} n_{avg}, \tag{1}$$

where v_p and v_{lc} are the filling factors of the polymer and LC in the composite, respectively. The n_{avg} is the average refractive index of LC, which can be expressed as $n_{avg} = (2n_o + n_e)/3$, where n_o and n_e are the ordinary and extraordinary refractive indices of the host LC, respectively, and n_p is the refractive index of the polymer matrix. In this case, the value of n_{avg} is greater than n_p, and the magnitude of n_i can vary between n_p and n_{avg} [30].

As electric fields are applied to the device, the LC directors with positive dielectric anisotropy ($\Delta\varepsilon > 0$) are reoriented along the field direction, resulting in the maximum induced birefringence. This phenomenon can be explained by the Kerr effect, written as $\Delta n_{ind} = K\lambda E^2$, where K is the Kerr constant, λ is the wavelength of the propagating beam, Δn_{ind} is the induced birefringence, and E is the applied electric field [33]. When a sufficient electric field is applied, the LC director of bipolar droplets are forced to follow periodic field lines, causing the refractive indices to change with the field strength. Therefore, the propagating beam interacts with synchronized specially modulated refractive indices with periodicity while transmitting through the device. In the present work, we discuss two switching modes: IPS (Fig. 1b) and VIS (Fig. 1c) modes. When IPS fields are applied between the P1 and P2 electrodes, the bipolar structured nano-sized LC droplets do not respond to the fields and remain invariant in region I because of the minimal field strength right over the electrodes. Therefore, the propagating beam experiences an effective refractive index, $n_{avg} \sim n_i$, as it passes through. In contrast, the VIS mode applies a constant offset voltage ($V_{offest} \neq 0$) to the electrode (P3) while maintaining the IPS fields between the electrodes (P1 and P2), resulting in vertical fields between the top and bottom (P1 and P2 to P3) and horizontal fields (P1 and P2) between the electrodes. Under this condition, the n_{avg} in Equation (1) is replaced by n_o. Consequently, n_i becomes n_o' as the polarized beam rotates parallel or perpendicular to the electrode direction because the LC directors are mostly reoriented in the vertical direction, that is, perpendicular to the substrate, owing to the stronger fields in region I. It can be noted in region I that the value of the refractive index n_o' in the VIS mode is relatively smaller than that of n_i in the IPS mode since $n_o < n_i$. In region II, the intensity of the horizontal field lines gradually increases from the center of region I to region III at the cost of the applied fields, contributing to the re-orientation of the LC directors preferably in the oblique directions in both cases. Therefore, the propagating beam experiences a refractive index change n', which can be defined as:

$$n' \sim v_p n_p + v_{lc} n_{eff} \tag{2}$$

$$n_{eff} = \left(\frac{n_o n_e}{\sqrt{n_o^2 \cos^2\theta + n_e^2 sin^2\theta}} \right), \tag{3}$$

where θ is the angle between the LC director and direction of the polarized incident beam [34]. When the direction of the incident beam is rotated perpendicular to electrodes, the polarized beam experiences a refractive index n_{eff}; however, the n_{eff} is greater than that of the value of n_o, that is, ($n_{eff} > n_o$). After substituting it to Equation (2), the values of the refractive index n' become n_{ips}' and

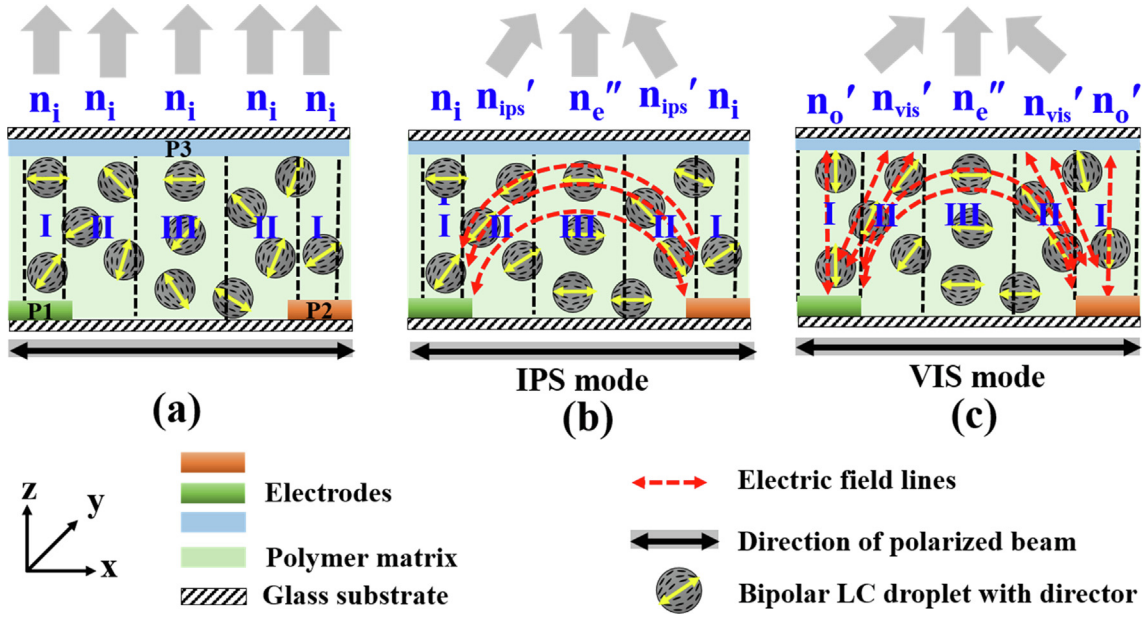

Fig. 1. Driving mechanism of the optically isotropic nano-PDLC for effective micro-lenticular lensing effect: (a) Random orientation of nano-sized bipolar LC droplets within a polymer matrix in the field-off state and reorientation of corresponding LC directors along the applied field direction in (b) IPS and (c) VIS modes with the change in effective refractive indices in each position and polarized direction of an incident beam kept along the x-direction.

n_{vis}' in the IPS and VIS modes, respectively. In region III, the intensity of the oblique field lines gradually decreases as they move towards regions II to III, and the horizontal fields become stronger in comparison to those in regions I and II owing to the inhomogeneous electric field distribution. As a result, the in-plane field tends to drive the LC directors through twist deformation aligned parallel to the electrode direction, that is, the x-axis, and the polarized beam experiences an effective refractive index n_e when the incident beam is adjusted perpendicular to the electrode direction. When the refractive index n_e is substituted in place of n_{eff} in Equation (2), the n' becomes n_e'' in both modes.

Considering the effective refractive index modulation between the interdigitated electrodes in relation to the applied field strength, the effective phase modulation ($\Delta\delta$) between regions I and III can be determined as [13,30,35]

$$\Delta\delta_{ips/vis} = \frac{2\pi}{\lambda}\left|\int_0^d (\text{Region III})(E)dz - (\text{Region I})d\right|, \quad (4)$$

where d and λ, are the film thickness and the wavelength of the transmitting beam. Herein, the refractive index variation between regions III and I is critical in determining the variation in $\Delta\delta$. Based on this, the magnitude of $\Delta\delta$ between regions III and I is given by $\Delta\delta_{ips/vis} = n_e'' - n_o'$ or $n_e'' - n_i$ for the VIS or IPS mode, respectively. This clearly shows that the VIS mode offers larger $\Delta\delta$ compared to that in the IPS mode because $n_o' < n_i$. The larger phase shift difference between region III and I could be responsible for obtaining the effective micro-lenticular lensing profile in the VIS mode. Because, the symmetric arrangement of the electrodes is responsible for the symmetric distribution of the field strength in the LC director profile, causing effective refractive index modulation from regions I to III. In this condition, when the transmitted beam is adjusted perpendicular to the electrode, the polarized beam interrelates with the effective gradient refractive indices $n_o' < n_{vis}' < n_e'' > n_{vis}' > n_o'$ and $n_i < n_{ips}' < n_e'' > n_{ips}' > n_i$ in regions I, II, III, II, and I for the VIS and IPS modes, respectively. Due to the contribution of symmetric refractive index modulation, we can achieve an ideal micro-lenticular lensing profile compared to that in the conventional IPS mode. In addition, assuming the uniaxial bipolar profile of the droplets under electric fields, the focal length (f) of the micro-lenticular lens device can be expressed as [36]

$$f_{ips/vis} = \frac{\pi w^2}{4\lambda(\Delta\delta_{ips/vis})} \quad (5)$$

where w is the width or pitch of the micro-lenticular aperture and $\Delta\delta_{ips/vis}$ is the phase change measured between the micro-lenticular lens centers (region III) and above the electrode (region I). According to Equation (4), the f_{vis} of the micro-lenticular lens is shorter owing to the larger value of $\Delta\delta_{vis}$. In practice, the $\Delta\delta$ is equal to $\delta\varphi = k \cdot d \cdot v_{lc} \cdot (n_e - n_o)/3$, where k is the wave vector ($2\pi/\lambda$) [28].

3. Experimental section

3.1. Materials

An optically isotropic nano-PDLC was prepared using a high-dielectric nematic LC, MLC2053 ($\Delta\varepsilon$ = 42.6, Δn = 0.235, and T_{NI} = 86 °C, Merck Advanced Technology, Korea), and a photocurable monomer, NOA-65 (Norland Optical Adhesive, n_p = 1.5122 at 20 °C and 589 nm). A small amount of a photoinitiator (Irgacure-907) was then added to this mixture to initiate radical polymerization upon ultraviolet (UV) light exposure. The composite mixture contained 42.5 wt% of LC, 57.3 wt% of NOA-65, and 0.2 wt% of Irgacure-907. No additional purification was conducted prior to employing the materials.

3.2. Fabrication of Micro-lenticular device

A two substrates i.e. an interdigitated IPS and a plane electrode was utilized and a uniform gap between the top and bottom substrates of the device was maintained by a 4 μm ball spacer in order to fabricate the proposed device. The interdigitated electrode configuration had a width (w) of 4 μm and a distance (l) of 4 μm between them. The composite mixture was heated above T_{NI} (90 °C) and stirred several times to obtain a homogeneous mixture and the resulting mixture was infiltrated into the fabricated cell via

capillary action. Subsequently, phase separation was achieved by exposing the device to UV light at an intensity of 120 mW/cm^2 for 6 min.

3.3. Characterization and measurements

Subsequently, we demonstrated a micro-lenticular lensing effect followed by the diffraction properties of our proposed design using a variety of characterization techniques. A polarizing optical microscope (POM) (Nikon, ECLIPSE E600, Japan) attached to a CCD camera (Nikon, DXM 1200) was used to observe the micro-lenticular lensing effect, as well as the phase behavior under the applied field with a function generator (Agilent 33521A). The change in the transmittance of an incident polarized beam in response to an applied voltage was used to determine the diffraction efficiency (D_f). The black screen was placed 72 cm away from the proposed device to achieve far-field diffraction, and subsequent diffraction images were captured using a high-resolution camera (Samsung, NX1000). Finally, the embedded LC molecules were extracted from the polymer film, and the morphology of the polymer network was examined using a field-emission scanning electron microscope (FESEM). The LC droplet size distribution was calculated using Image J software.

4. Results and discussion

4.1. Surface morphological studies

Fig. 2 depicts an FESEM micrograph of the polymer morphology used to investigate the droplet size distribution of the network. Several holes in the micrograph that had previously been occupied by the LC molecules were observed. The FESEM image was captured after successful elimination of the LC molecules from the polymer network by soaking the sample device in an n-hexane solution for two days [37,38]. Fig. 2a shows a continuous network of the polymer matrix appeared throughout the active surface area of the device with a uniform distribution of droplet holes. Fig. 2b shows the relative droplet size distribution of the micrograph which was statistically estimated using the Image J software. The droplet size distribution implies that all droplet sizes appear to be less than the wavelength of visible light, that is, <300 nm, and the estimated mean droplet size is approximately 188 nm. A few droplets with irregular shapes are also observed in the FESEM micrograph, which can be attributed to the UV light exposure at higher intensities. Obtained symmetrical or asymmetrical shape of the LC droplets does not deteriorate the physical properties or phase modulation of the device either in bending or twisting mode because the size of the droplet is smaller than the wavelength of visible light [26]. Furthermore, the estimated v_{lc} value is 18.45%, which is lower than the concentration of LC used in the experiment because of inadequate removal of LC as the LC molecules dissolve and surround the polymer network [32,39,40]. Herein, the v_{lc} is defined as the ratio of the area of the LC droplets in the polymer matrix to the total area of the captured FESEM micrograph [28].

4.2. Polarizing optical microscopy

Fig. 3 illustrates the POM images of the micro-lenticular device captured under various driving schemes such as the IPS and VIS modes. In the field-off state, the micro-lenticular device appears dark in color and remains invariant when the sample plane is rotated between the crossed polarizers, as shown in Fig. 3a. In addition, a high-resolution photographic image of the micro-lenticular device is displayed in the inset of Fig. 3a. The photographic image was captured at the ambient light condition without

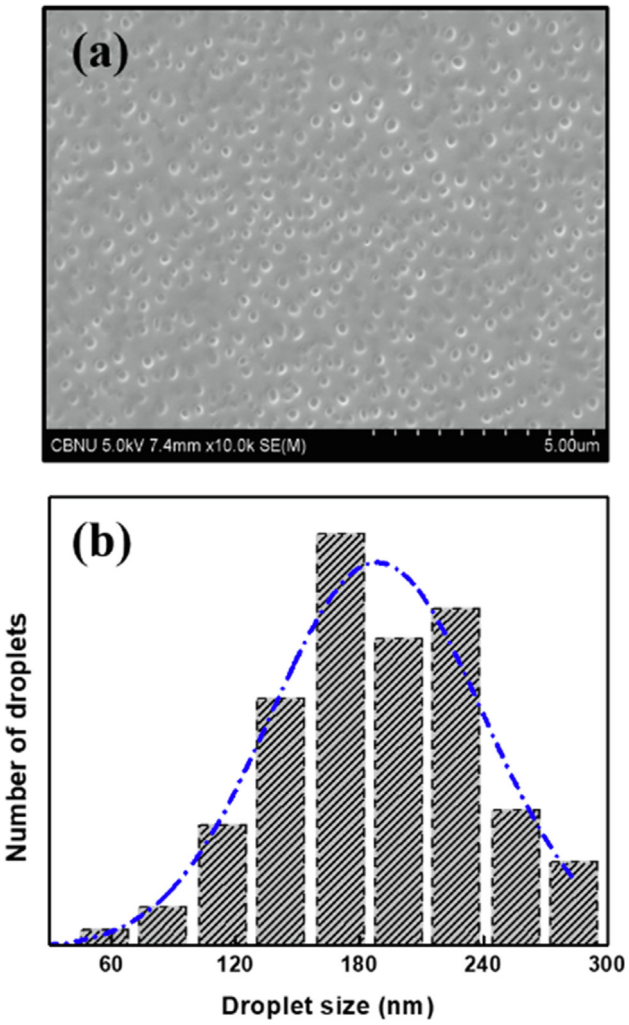

Fig. 2. (a) FESEM image of the LC removed polymer matrix of the nano-PDLC and (b) Size distribution of the LC droplets in the continuous polymer matrix.

attaching the polarizers and external field to the device. As it is highly transparent, the image "*ID LAB*" under the device did not experience phase retardation while passing through the birefringent film [31,41]. Due to the reason, the photographic image demonstrates that the image "*ID LAB*" under the device is clearly visible to the human eye [26,30].

To realize the induced phase retardation, the ITO electrodes of the device were adjusted to 45° to the transmission axis of the polarizer and analyzer. When sufficient fields were applied to a device, maximum birefringence was induced by reorienting the LC directors in the applied field direction. As a result, the device exhibited periodic bright and dark fringe patterns as the polarizers were crossed, as shown in Fig. 3a,b. Dark fringe patterns in region I appeared in both modes. In the IPS mode, the LC directors unchanged and remain as n_{avg} owing to the low intensity of the field strength, therefore we realize no phase retardation. In the VIS mode, the phase modulation occurred by reorienting the LC directors in a direction perpendicular to the substrate from a random direction, i.e. the refractive index changed to n_o' from the n_{avg} owing to strong longitudinal electric fields. In addition, we notice a thick dark fringe pattern in the VIS mode over the electrodes as compared to the dark fringe in the IPS mode, corresponding to vertically aligned LC droplets up to the edge of the electrodes as homeotropic alignment-based conventional LC devices. Moving to the non-electrode region, the brightness intensity appeared to

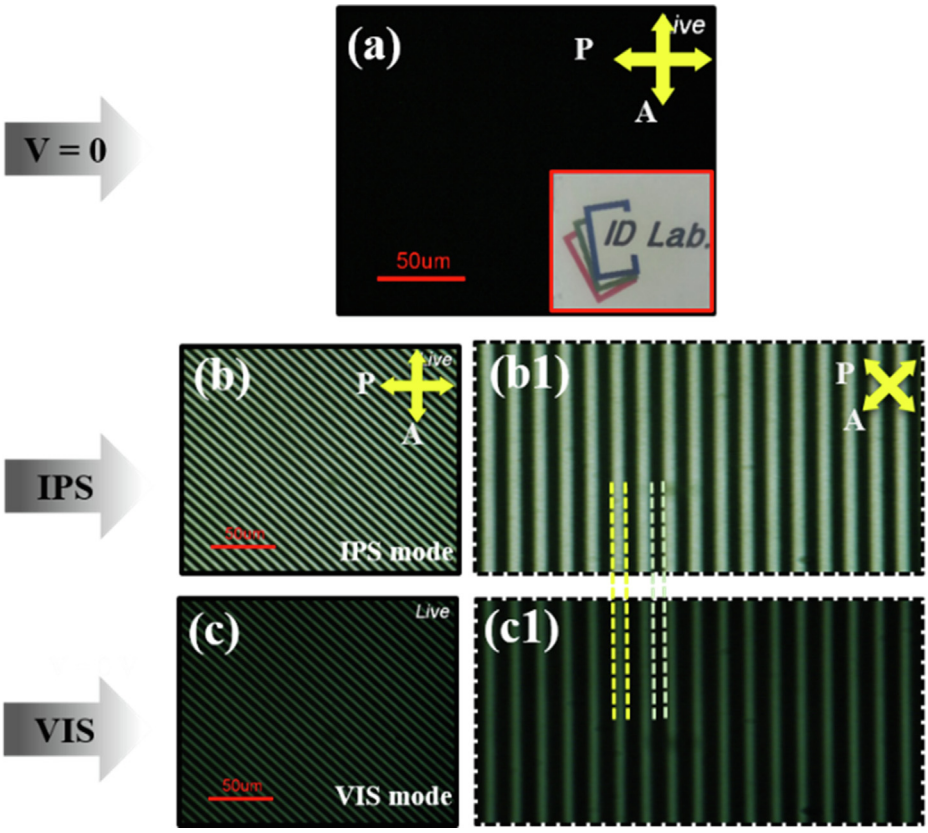

Fig. 3. Polarized optical micrographs of optically isotropic nano-PDLC: (a) Field-off state (V = 0 V), (b) IPS (V_{ac} = 50 V) and (c) VIS (V_{ac} = 50 V, V_{offset} = 20 V) mode with the applied square wave frequency of 1 kHz and its corresponding enlarged images on their right side. The photographic image of the micro-lenticular lens device depicted in the inset is captured above the word "***ID LAB***".

be uniform between the electrodes, that is, regions II and III in the IPS mode, but non-uniform transmittance was realized in the VIS mode. Although the transmittance intensity was high in the IPS mode, a line-type sharp transmittance between the interdigitated electrodes was noticed in the VIS mode manifesting ideal like micro-lenticular lensing profile owing to the increase in the field strength from region II to III. The difference in width of the bright and dark fringes is illustrated by the dotted lines in enlarged Fig. 3b1,c1. The experimental results show a clear increase or decrease of transmittance between electrodes, confirming that the most effective graded refractive index is achieved because of the implemented VIS mode.

Fig. 4a shows a schematic diagram of the optical microscope used to estimate the focal length f of the micro-lenticular lens arrays. The bright and dark fringe lines that appeared under the crossed polarizers remained in the same position when the analyzer was withdrawn. The polarized beam was then adjusted perpendicular to the electrode direction by retaining the bright focus lines at the same place. In this situation, the polarized beam was focused by interacting with the interface of the graded refractive indices of the nano-sized LC droplets from one edge of the electrode to another, that is, regions I, II, III, II, and I in the order of n_i <- n'_{ips} < n''_e > n'_{ips} > n_i and n_o' < n'_{vis} < n''_e > n'_{vis} > n_o' for the IPS and VIS modes, respectively. This was because of electric field inhomogeneity. Furthermore, in both cases, the horizontal field strength gradually increased from the middle of the electrode to the center between the interdigitated electrodes (region III). Herein, the focal lines of the micro-lenticular lens were determined as the maximum intensity of the focused beam in region III. The periodic focal lines of the micro-lenticular lens are displayed between the white dotted lines drawn in the enlarged image of Fig. 4b. The resulting transmittance interference fringe focal line distribution of the IPS and VIS micro-lenticular lens measured with respect to the electrode distance were shown in Fig. 4c. This manifests that the experimentally measured transmittance of VIS mode data possesses ideal lens-like phase profiles as compared to that of the conventional IPS mode. Besides, the circular solid one in inset of Fig. 4c depicts that the measured transmittance while the dashed rea line represents the parabolic fitting, which confirms that the data fits well with the fitting. Herein, the focal length f is defined as the distance between the electrode on the substrate and the position of the focal lines that appear at the focal plane. At a fixed applied field, the measured f of the micro-lenticular lens are 46 and 38 μm for the IPS and VIS modes, respectively. The experimentally estimated f of the micro-lenticular lens is ∼ 35 μm, which is obtained by substituting the value of the phase shift $\delta\varphi$. The $\delta\varphi$ is estimated using the relationship $\delta\varphi = 2\pi/\lambda \cdot d \cdot \nu_{lc} \cdot (n_e - n_o)$ / 3 [28], where the value of ν_{lc} is obtained from the FESEM micrograph shown in Fig. 2(a). The experimental results confirm that the proposed VIS mode provides a higher $\Delta\delta_{vis}$ owing to a larger magnitude of the refractive index change, that is, $n''_e - n_o'(\Delta\delta_{vis}) > n''_e - n_{avg}$ $(\Delta\delta_{ips})$. Despite the fact that the $\Delta\delta_{vis}$ is larger in the VIS mode, this mode provides a better micro-lenticular lensing profile and a lower f than that in the conventional IPS mode because the $\Delta\delta$ and f are inversely proportional to one another. The proposed device features a short f_{vis} that has the potential to contribute to an improvement in the image resolution.

Furthermore, we investigate the polarization-dependent micro-lenticular lensing effect by establishing focal lines between the interdigitated electrodes, that is, region III. Fig. 5 shows the change in the position of the focal lines between the white dotted lines as the direction of the polarized beam change. According to the earlier

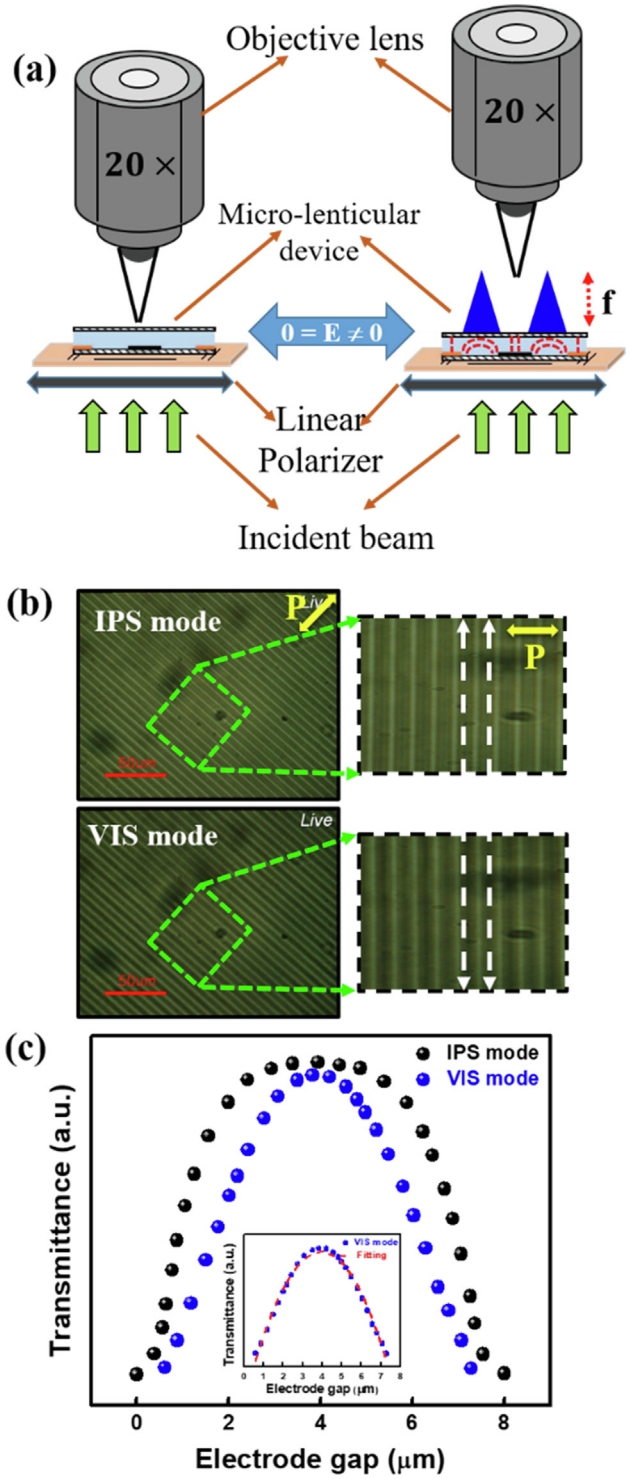

Fig. 4. (a) Experimental setup for measuring focal length (b) Optical images of the focal lines (c) Transmittance intensity profiles of the micro-lenticular lens with respect to electrode distance with incident polarized beam positioned perpendicular to the electrode direction. The inset shows the measured VIS mode transmittance data with parabolic fitting.

discussion, the proposed VIS mode displays focal lines in region III, as the polarized beam is adjusted perpendicular to the electrode direction. However, the position of the focal lines switches from bright to dark as the polarized beam rotates from the perpendicular to the parallel electrode direction. The incident polarized beam experiences refraction at the interface of the effective graded

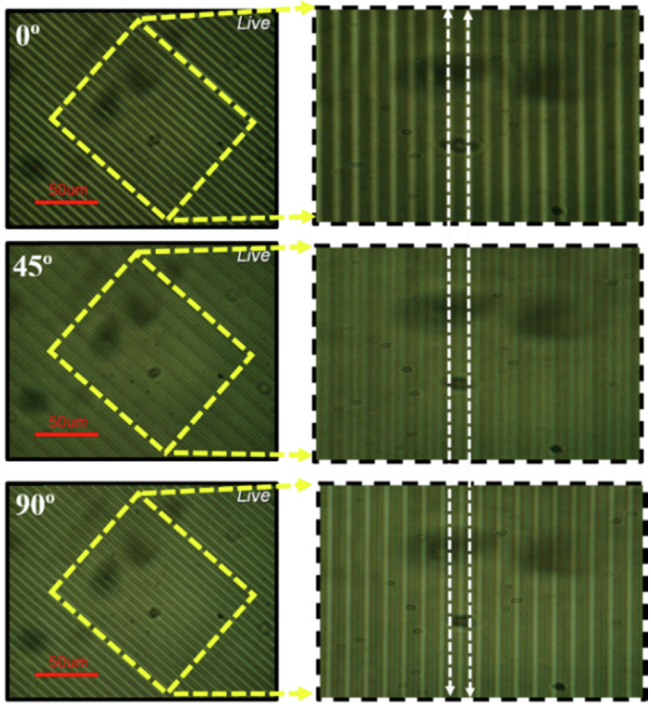

Fig. 5. Focal lines of the proposed VIS mode micro-lenticular lens that change with respect to electrode direction as the incident polarized beam is rotated at 0°, 45°, and 90°.

refractive index in the order of $n_o' < n_{vis}' < n_e'' > n_{vis}' > n_o'$ to $n_o' > n_{vis}' > n_e'' < n_{vis}' < n_o'$ in regions I, II, III, II, and I, respectively, which causes a deviation in the incident beam path. The obtained experimental results clearly show that the proposed device functions as a polarization-dependent micro-lenticular lens. Similar observations were demonstrated with optically isotropic nano-PDLC in an earlier study with no plane electrode on the top substrate [30]; in this case, however, the phase difference between region I and III was relatively low. In addition, a few other polarization-dependent micro-lenticular lenses based on ferroelectric LC [42], index matching between polymer arrays and LC [43,44], polymer network LC [45], PVC, and PVC/DBP gel [46,47] have been reported in the literature. However, these micro-lenticular lensing devices require intricate fabrication and exhibit LC deformation in response to external pressure.

4.3. Diffraction properties

Fig. 6a depicts an experimental ray diagram for measuring the diffraction efficiency (D_f) of the proposed micro-lenticular device. A polarizer was used to direct the propagating beam perpendicular to the electrode direction, and a block screen was placed behind the micro-lenticular device to identify the beam intensity variation. In the field-off state, the higher diffraction ($\pm 1^{st}$ and $\pm 2^{nd}$) orders were realized due to the refractive index mismatch between the ITO and non-ITO region, however, in our case, the intensity of higher diffraction orders were controlled by placing a ND filter in front of the polarizer. The beam intensity of the diffraction orders could be detected using a photodetector connected to an oscilloscope. Fig. 6b shows the high-resolution photographic diffraction patterns of the IPS and VIS modes. As the incident beam propagated through the device, no diffraction effect was observed in the field-off state because the proposed device exhibits an optically isotropic phase n_i. For this reason, the 0^{th} order of beam intensity was relatively high when compared to the higher diffraction orders

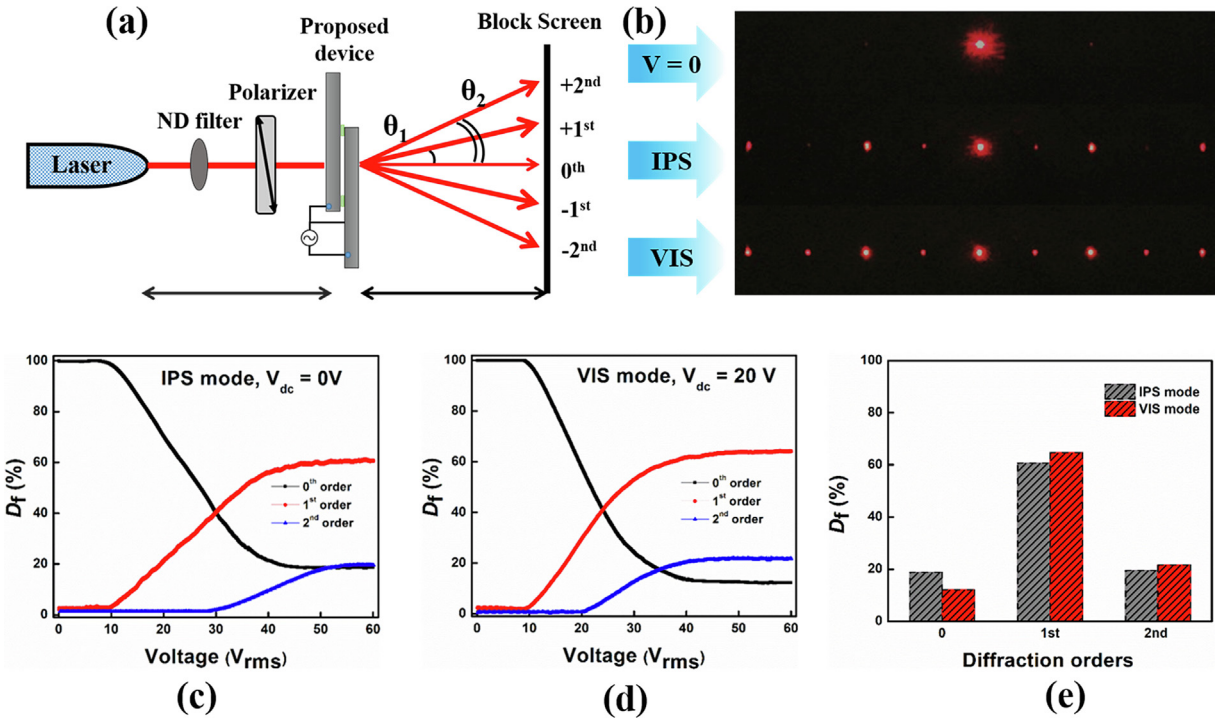

Fig. 6. (a) Experimental setup for diffraction efficiency (D_f) measurement of the proposed micro-lenticular device (b) Photographic images of the diffraction patterns at the voltage-off and −on states (c, d) Voltage-dependent diffraction efficiencies for the IPS and VIS modes, respectively. (e) Comparative diffraction efficiencies of the IPS and VIS modes. Diffraction efficiencies are referred to as both + ve and −ve sides of the first and second orders. The wavelength of the incident beam is 633 nm.

that appear on either side of the 0th order. When the IPS and VIS modes are operated, the periodic phase modulation occurs between electrodes owing to the redirection of the LC directors along the field direction. Consequently, the intensity of the 0th order gradually decreases and deviates symmetrically to the higher orders because the polarized beam experiences different refractive indices in the order of $n_i < n'_{ips} < n''_e > n'_{ips} > n_i$ and $n_o' < n'_{vis} < n''_e > n'_{vis} > n_o'$ in regions I, II, III, II, and I, respectively, while propagating between the active electrode and non-electrode regions [48,49]. Herein, the D_f is measured as the ratio of the m^{th} order to the 0th order beam intensity. The D_f can be expressed as

$$D_f = \frac{I_m(V \neq 0)}{I_0(V = 0)} \times 100, \quad (6)$$

where $I_m(V \neq 0)$ is the m^{th}-order beam intensity at the applied voltage, and $I_0(V = 0)$ is the 0th order intensity at zero voltage ($V = 0$). The diffraction angles are calculated using the well-known trigonometric equation: $tan\ \theta_m = D_m/L$, where D_m is the distance between the 0th and m^{th} diffraction orders and L is the distance between the sample device and the block screen. Fig. 6c,d display the D_f as a function of the applied voltages for the IPS and VIS modes, respectively. As the applied fields are increased, the 0th order intensity is gradually transferred symmetrically to either side of the higher diffraction orders. It is worth noting that the overall D_f of the 0th order intensity in the VIS mode is nearly ~ 6.7% higher than that in the IPS mode. In addition, it also shows a higher D_f by ~ 4% and 2% for ± the 1st and ± 2nd orders, respectively, when compared to the IPS mode. Table 1 summarizes the measured diffraction efficiencies and diffraction angles of the IPS and VIS modes. The overall increase in D_f is attributed to the larger $\Delta\delta$ in the VIS mode, that is $\Delta\delta_{vis} > \Delta\delta_{ips}$. Additionally, the obtained D_f values are in good agreement with those reported in previous studies [13,26]. Furthermore, the diffraction angles remain consistent because the pitch length Λ is same in both cases. It should also be noted that the obtained diffraction angles agree well with the theoretical equation $sin\theta_m = m\lambda/n_{avg}\Lambda$, where θ_m is the diffraction angle.

5. Conclusions

Herein, we successfully developed an electrically tunable effective phase modulation of a transparent polymer/LC composite film for micro-lenticular lens and diffractors by implementing the VIS mode. The fabricated device is optically transparent in the visible wavelength regime due to optically isotropic behavior and the phase remain invariant in the field-off state. The proposed micro-lenticular device exhibits phase modulation even above the electrodes as a result of reorienting the nano-sized LC droplets by utilizing a vertical electric field with three terminals. The polarized

Table 1
Diffraction efficiency (D_f) and diffraction angle (θ) of the IPS and VIS modes.

Diffraction order	D_m (cm)	IPS			VIS		
		D_f (%)	θ (°)	θ (°)*	D_f (%)	θ (°)	θ (°)*
0th	–	18.82	–	–	12.14	–	–
1st	6.9	60.73	5.47	5.57	64.68	5.47	5.57
2nd	14	19.58	11.0	11.19	21.66	11.0	11.19

* Theoretically measured diffraction angle.

optical and optical images clearly demonstrate that the proposed mode generates phase modulation in both regions between and over the electrodes. With the proposed VIS mode, we accomplish a larger phase modulation between region I and III and enables a better micro-lenticular lensing profile and well matches with an ideal like lens as compared to that of conventional IPS mode. However, it has a focal length of 38 μm, which is relatively shorter than that of the conventional micro-lenticular lens driven under IPS fields despite this still capable of achieving images with high-resolution. Furthermore, the proposed optically isotropic nano-PDLC device functions as a switchable diffraction grating with higher diffraction efficiencies for the 0^{th}, 1^{st}, and 2^{nd} diffraction orders than those in the IPS mode.

CRediT authorship contribution statement

Srinivas Pagidi: Conceptualization, Methodology, Resources, Investigation, Data curation, Validation, Writing – original draft. **MinSu Kim:** Visualization, Writing – review & editing. **Ramesh Manda:** Visualization, Writing – review & editing. **Soyeon Ahn:** Formal analysis. **Min Yong Jeon:** Conceptualization, Visualization, Writing – review & editing, Supervision. **Seung Hee Lee:** Formal analysis, Conceptualization, Visualization, Writing – review & editing, Supervision.

Data availability

Data will be made available on request.

Declaration of Competing Interest

The authors declare that they have no known competing financial interests or personal relationships that could have appeared to influence the work reported in this paper.

Acknowledgment

This research was supported by the Basic Science Research Program through the National Research Foundation of Korea (NRF) funded by the Ministry of Science and ICT (NRF-2019R1A2C1084933, NRF-2019R1A5A8080326, NRF-2020R1A6A1A03047771, NRF-2021R1I1A1A01060001, NRF-2022R1A2C2091671); by a Korea Institute for Advancement of Technology (KIAT) grant funded by the Korea Government (MOTIE) (P0008458, The Competency Development Program for Industry Specialist).

References

[1] E. Lueder, Liquid crystal displays: Addressing Schemes and Electro-Optical Effects (2001) Chichester, Wiley, West Sussex, U.K.
[2] S. Zimmerman, K. Beeson, M. McFarland, J. Wilson, T. Credelle, K. Bingaman, P. Ferm, J. Yardley, Viewing-angle-enhancement system for LCDs, J. Soc. Inf. Disp. 3 (1995) 173.
[3] A. Shibukawa, A. Okamoto, M. Takabayashi, A. Tomita, Spatial cross modulation method using a random diffuser and phase-only spatial light modulator for constructing arbitrary complex fields, Opt. Express 22 (2014) 3968.
[4] S. Sato, A. Sugiyama, R. Sato, Variable-focus liquid-crystal Fresnel lens, Jpn. J. Appl. Phys. 24 (8A) (1985) L626.
[5] T. Matsui, R. Ozaki, K. Funamoto, M. Ozaki, K. Yoshino, Flexible mirrorless laser based on a free-standing film of photopolymerized cholesteric liquid crystal, Appl. Phys. Lett. 81 (2002) 3741.
[6] J. Arines, Impact of liquid crystals in active and adaptive optics, Mater. 2 (2009) 549.
[7] E. Otón, J. Pérez-Fernández, D. López-Molina, X. Quintana, J.M. Otón, M.A. Geday, Reliability of liquid crystals in space photonics, IEEE Photonics J. 7 (2015) 1.
[8] S.-T. Wu, H. Ren, Introduction to adaptive lenses, John Wiley & Sons, 2012.
[9] J.F. Algorri, D.C. Zografopoulos, V. Urruchi, J.M. Sánchez-Pena, Recent advances in adaptive liquid crystal lenses, Crystals 9 (2019) 272, https://doi.org/10.3390/cryst9050272.
[10] N.-T. Nguyen, Micro-optofluidic Lenses: A review, Biomicrofluidics 4 (3) (2010) 031501.
[11] Y.-H. Lin, Y.-J. Wang, V. Reshetnyak, Liquid crystal lenses with tunable focal length, Liq. Cryst. Rev. 5 (2017) 111.
[12] Y.-J. Wang, P.-J. Chen, X. Liang, Y.-H. Lin, Augmented reality with image registration, vision correction and sunlight readability via liquid crystal devices, Sci. Rep. 7 (2017) 1.
[13] R. Manda, S. Pagidi, S.S. Bhattacharyya, C.H. Park, Y.J. Lim, J.S. Gwag, S.H. Lee, Fast response and transparent optically isotropic liquid crystal diffraction grating, Opt. Express 25 (2017) 24033.
[14] M.P.C.M. Krijn, S.T. de Zwart, D.K.G. de Boer, O.H. Willemsen, M. Sluijter, 2- D/3- D displays based on switchable lenticulars, J. Soc. Inf. Disp. 16 (2008) 847, https://doi.org/10.1889/1.2966446.
[15] H. Ren, S. Xu, Y. Liu, S.-T. Wu, Switchable focus using a polymeric lenticular microlens array and a polarization rotator, Opt. Express 21 (2013) 7916.
[16] C.-W. Chen, Y.-P. Huang, P.-C. Chen, Dual direction overdriving method for accelerating 2D/3D switching time of liquid crystal lens on auto-stereoscopic display, J. Disp. Tech. 8 (2012) 559.
[17] J. Flack, J. Harrold, G.J. Woodgate, A prototype 3D mobile phone equipped with a nextgeneration autostereoscopic display, Stereoscopic Displays and Virtual Reality Systems XIV, Int. Soc. Opt. Photonics (2007) 64900M.
[18] N.S. Holliman, N.A. Dodgson, G.E. Favalora, L. Pockett, Three-dimensional displays: a review and applications analysis, IEEE Trans. Broadcasting 57 (2011) 362.
[19] B. Lee, J.-H. Park, Overview of 3D/2D switchable liquid crystal display technologies, Emerging Liquid Crystal Technologies, Emerging Liquid Crystal Technologies V, International Society for Optics and Photonics, 2010, p. 761806.
[20] J. Kim, J. Kim, J.-H. Na, B. Lee, S.-D. Lee, Liquid crystal-based square lens array with tunable focal length, Opt. Express 22 (2014) 3316.
[21] H. Dou, F. Chu, Y.-Q. Guo, L.-L. Tian, Q.-H. Wang, Y.-B. Sun, Large aperture liquid crystal lens array using a composited alignment layer, Opt. Express 26 (2018) 9254.
[22] C.-J. Hsu, J.-J. Jhang, C.-Y. Huang, Large aperture liquid crystal lens with an imbedded floating ring electrode, Opt. Express 24 (2016) 16722.
[23] S.-G. Kang, J.-H. Kim, Optically-isotropic nanoencapsulated liquid crystal displays based on Kerr effect, Opt. Express 21 (2013) 15719, https://doi.org/10.1364/OE.21.015719.
[24] M.S. Kim, Y.J. Lim, S. Yoon, S.-W. Kang, S.H. Lee, M. Kim, S.-T. Wu, A controllable viewing angle LCD with an optically isotropic liquid crystal, J. Phy. D Appl. Phys. 43 (2010).
[25] C.H. Park, E.J. Shin, R. Manda, S.C. Noh, M.-H. Lee, S.H. Lee, Fast Response and Scattering Free Optically Isotropic Liquid Crystal Device for Flexible Display Applications, SID Symposium Digest of Technical Papers, Wiley Online Library, 2016, p. 1506-1508.
[26] R. Manda, S. Pagidi, Y.J. Lim, R. He, S.M. Song, J.H. Lee, G.-D. Lee, S.H. Lee, Self-supported liquid crystal film for flexible display and photonic applications, J. Mol. Liq. 291 (2019), https://doi.org/10.1016/j.molliq.2019.111314.
[27] J.L. West, Phase separation of liquid crystals in polymers, Mol. Crys. Liq. Crys. Inc., Nonlinear Opt. 157 (1) (1988) 427–441.
[28] J.H. Yu, H.-S. Chen, P.-J. Chen, K.H. Song, S.C. Noh, J.M. Lee, H. Ren, Y.-H. Lin, S.H. Lee, Electrically tunable microlens arrays based on polarization-independent optical phase of nano liquid crystal droplets dispersed in polymer matrix, Opt. Express 23 (2015) 17337.
[29] H. Ren, Y.-H. Fan, Y.-H. Lin, S.-T. Wu, Tunable-focus microlens arrays using nanosized polymer-dispersed liquid crystal droplets, Opt. Commun. 247 (2005) 101.
[30] S. Pagidi, R. Manda, S.S. Bhattacharyya, S.G. Lee, S.M. Song, Y.J. Lim, J.H. Lee, S.H. Lee, Fast Switchable Micro-Lenticular Lens Arrays Using Highly Transparent Nano-Polymer Dispersed Liquid Crystals, Adv. Mater. Interfaces 6 (2019) 1900841, https://doi.org/10.1002/admi.201900841.
[31] S. Pagidi, R. Manda, Y.J. Lim, S.M. Song, H. Yoo, J.H. Woo, Y.-H. Lin, S.H. Lee, Helical pitch-dependent electro-optics of optically high transparent nano-phase separated liquid crystals, Opt. Express 26 (2018) 27368.
[32] Y.J. Lim, J.H. Yoon, H. Yoo, S.M. Song, R. Manda, S. Pagidi, M.-H. Lee, J.-M. Myoung, S.H. Lee, Fast switchable field-induced optical birefringence in highly transparent polymerliquid crystal composite, Opt. Mater. Express 8 (2018) 3698.
[33] J. Kerr, Xl., A new relation between electricity and light: Dielectrified media birefringent, The London, Edinburgh, and Dublin, Philosophical Magazine and Journal of, Science 50 (1875) 337, https://doi.org/10.1080/14786447508641302.
[34] D.-K. Yang, S.-T. Wu, Fundamentals of liquid crystal devices, John Wiley & Sons, 2014.
[35] J. Yan, Y. Xing, Q. Li, Dual-period tunable phase grating using polymer stabilized blue phase liquid crystal, Opt. Lett. 40 (2015) 4520.
[36] Y.-H. Lin, H.-S. Chen, H.-C. Lin, Y.-S. Tsou, H.-K. Hsu, W.-Y. Li, Polarizer-free and fast response microlens arrays using polymer-stabilized blue phase liquid crystals, Appl. Phys. Lett. 96 (2010).
[37] S. Pagidi, R. Manda, S.S. Bhattacharyya, K.J. Cho, T.H. Kim, Y.J. Lim, S.H. Lee, Superior electro-optics of nano-phase encapsulated liquid crystals utilizing functionalized carbon nanotubes, Compos. B Eng. 164 (2019) 675.

[38] S. Pagidi, H. Park, D. Lee, M. Kim, S.H. Lee, Nanosize-confined nematic liquid crystals at slippery interfaces of polymer composites consisting of poly (hexyl methacrylate), J. Mol. Liq. 350 (2022).
[39] C.-M. Chang, Y.-H. Lin, V. Reshetnyak, C.H. Park, R. Manda, S.H. Lee, Origins of Kerr phase and orientational phase in polymer-dispersed liquid crystals, Opt. Express 25 (2017) 19807.
[40] S. Pagidi, K.S. Pasupuleti, M. Reddeppa, S. Ahn, Y. Kim, J.-H. Kim, M.-D. Kim, S.H. Lee, M.Y. Jeon, Resistive type NO2 gas sensing in polymer-dispersed liquid crystals with functionalized-carbon nanotubes dopant at room temperature, Sens. Actuators B: Chem. 370 (2022) 132482.
[41] S. Pagidi, R. Manda, H.S. Shin, J. Lee, Y.J. Lim, M. Kim, S.H. Lee, Enhanced electro-optic characteristics of polymer-dispersed nano-sized liquid crystal droplets utilizing PEDOT: PSS polymer composite, J. Mol. Liq. 322 (2021).
[42] L. Shi, A.K. Srivastava, A.M.W. Tam, V.G. Chigrinov, H.S. Kwok, 2D–3D switchable display based on a passive polymeric lenticular lens array and electrically suppressed ferroelectric liquid crystal, Opt. Lett. 42 (2017) 3435, https://doi.org/10.1364/OL.42.003435.
[43] J. Kim, S.-U. Kim, B.-Y. Lee, J.-H. Suh, S.-D. Lee, Lenticular lens array based on liquid crystal with a polarization-dependent focusing effect for 2D–3D image applications, J. Inf. Disp. 16 (2015) 11.
[44] H. Kim, J. Kim, J. Kim, B. Lee, S.-D. Lee, Liquid crystal-based lenticular lens array with laterally shifting capability of the focusing effect for autostereoscopic displays, Opt. Commun. 357 (2015) 52.
[45] X. Wang, H. Ren, Q. Wang, Polymer network liquid crystal (PNLC) lenticular microlens array with no surface treatment, J. Disp. Tech. 12 (2016) 773.
[46] C. Lan, Z. Zhou, H. Ren, S. Park, S.H. Lee, Fast-response microlens array fabricated using polyvinyl chloride gel, J. Mol. Liq. 283 (2019) 155.
[47] M. Xu, B. Jin, R. He, H. Ren, Adaptive lenticular microlens array based on voltage-induced waves at the surface of polyvinyl chloride/dibutyl phthalate gels, Opt. Express 24 (2016) 8142.
[48] J. Yan, Y. Li, S.-T. Wu, High-efficiency and fast-response tunable phase grating using a blue phase liquid crystal, Opt. Lett. 36 (2011) 1404.
[49] Y. Hori, K. Asai, M. Fukai, Field-controllable liquid-crystal phase grating, IEEE Trans. Electron Dev. 26 (11) (1979) 1734–1737.